The Journal of Experimental Biology 211, 1120-1130
Published by The Company of Biologists 2008
doi:10.1242/jeb.010413

Kinematics and power requirements of ascending and descending flight in the pigeon (*Columba livia*)

Angela M. Berg* and Andrew A. Biewener

Harvard University, Concord Field Station, Department of Organismic and Evolutionary Biology, 100 Old Causeway Road, Bedford, MA 01730, USA

*Author for correspondence (e-mail: amberg@fas.harvard.edu)

Accepted 4 February 2008

SUMMARY

Ascending or descending locomotion involves a change in potential energy (*PE*) and a corresponding change in power requirement. We sought to test whether the mechanical power required for steady ascending or descending flight is a simple sum of the power required for level flight and the power necessary for potential energy change. Pigeons (*Columba livia*) were trained to fly at varying angles of ascent and descent (60°, 30°, 0°, –30°, –60°), and were recorded using high-speed video. Detailed three-dimensional kinematics were obtained from the recordings, allowing analysis of wing movement. Aerodynamic forces and power requirements were then estimated from kinematic data. As expected, '*PE* flight power' increased significantly with angle of flight (0.234 W deg.$^{-1}$), though there appeared to be a limit on the amount of *PE* that the birds could gain or dissipate per wingbeat. We found that the total power output for flight at various angles was not different from the sum of power required for level flight and the *PE* rate of change for a given angle, except for the steep –60° descent. The total power for steep descent was higher than this sum because of a higher induced power due to the bird's deceleration and slower flight velocity. Aerodynamic force estimates during mid-downstroke did not differ significantly in magnitude or orientation among flight angles. Pigeons flew fastest during –30° flights (4.9±0.1 m s^{-1}) and slowest at 60° (2.9±0.1 m s^{-1}). Although wingbeat frequency ranged from 6.1 to 9.6 Hz across trials, the variation was not significant across flight angles. Stroke plane angle was more horizontal, and the wing more protracted, for both +60° and –60° flights, compared with other flight path angles.

Supplementary material available online at http://jeb.biologists.org/cgi/content/full/211/7/1120/DC1

Key words: flight, incline, kinematics, pigeon, power.

INTRODUCTION

While in flight, a bird often needs to adjust its altitude. Changing altitude may be necessary to land, forage, pursue prey, or to maneuver through the environment. As with terrestrial locomotion, an increase in elevation during flight results in a change in the potential energy of the animal's center of mass. But unlike terrestrial animals, a bird in flight cannot push against a solid substrate to change its altitude. Instead, a bird must depend on interactions between its wings, tail and body and the air to effect this change.

Whereas the mechanics and energetics of incline locomotion have been fairly well studied in terrestrial animals (e.g. Gillis and Biewener, 2002; Dutto et al., 2004; Higham and Jayne, 2004), including humans (Iversen and McMahon, 1992; Gottschall and Kram, 2005; Roberts and Belliveau, 2005), and birds performing terrestrial locomotion (Bundle and Dial, 2003; Daley and Biewener, 2003; Gabaldon et al., 2004; Rubenson et al., 2006), there has been relatively little focus on the ascending and descending flight of birds. Past work has examined *in vivo* muscle function of birds during vertical or angled take-off and landing (Dial, 1992; Dial and Biewener, 1993; Askew et al., 2001). However, the kinematics and aerodynamic mechanisms underlying steady ascending and descending avian flight have remained largely unexplored.

In contrast to weight support during terrestrial locomotion, a bird, even when hovering and remaining stationary, must continually force air downward with its wings to support its weight (e.g. Norberg, 1990). Staying in place during flapping flight thus requires mechanical power. Freely hovering hummingbirds, for example, show a whole-body power output ranging from 22 to 38 W kg^{-1} (Altshuler et al., 2004). Steady, level, forward flight likewise requires power output, though there is no net change in kinetic or potential energy over the course of a wingbeat. Many studies have explored the relationship between forward flight speed and power output, with the goal of assessing whether birds display a U-shaped power curve and how differences in wing shape and flight style might affect this relationship (e.g. Torre-Bueno and Larochelle, 1978; Rothe et al., 1987; Rayner, 1999; Tobalske et al., 2003; Bundle et al., 2007).

Another straightforward way to explore differences in power output is to require a bird to change its potential energy by having it fly along an ascending or descending path. The main goal of the present study was to begin to explore how flight power requirements change as a function of flight path angle, by examining the free flight of pigeons trained to fly over varying angles of ascent and descent. In particular, we sought to determine whether the power required for incline or decline flight could be measured by simply summing the power necessary for level flight at the same speed and the rate of center of mass (CoM) potential energy change. Given our hypothesis that this would be the case, we expected to find that, compared to level flight, ascending flight would require more power, descending flight would require less power, and the difference in each case would be the rate of CoM potential energy change.

We also sought to explore how the direction and magnitude of average aerodynamic force produced by the wings during

downstroke changes with flight angle. Relative to level flight, we expected that aerodynamic force would be greater or rotated upward for climbing flight, as either alteration would result in an increased upward component of aerodynamic force.

By studying the kinematics of pigeons during ascending and descending flight, we sought to determine patterns of wing motion that might underlie differences in power and force between level and angled flight. We expected angle of attack to be determined primarily by the orientation of the incident velocity, which is largely influenced by the angle of flight. We thus expected to observe lower angles of attack for ascending flights and greater angles of attack for descending flights. Given that ascending flight would require a greater power output and descending flight a lower power output than level flight at a given speed, we also expected to observe greater wingbeat frequency for ascending flights, and lower wingbeat frequency for descending flights. We did not expect flight speed or stroke plane angle to vary among flight angles, as the size of our experimental flight arena did not allow for fast flight. Because of the relatively slow flight speed used by the pigeons in our experiments, the wingstroke would primarily need to direct airflow downward to support the bird's weight, suggesting that the stroke plane angle would be nearly horizontal for all conditions.

MATERIALS AND METHODS

Animals and experimental setup

Four rock pigeons *Columba livia* Linnaeus (hereafter 'pigeons'; Table 1) from a small flock housed at the Concord Field Station were used in the experiments. These pigeons were bred on-site from carrier pigeon stock. Birds were provided with food and water *ad libitum*. Body mass and wing data for each bird are shown in Table 1. Two wooden perches (one 22×62×2 cm and another slightly larger, 30×50×2 cm, covered with cardboard, thin plastic and paper towels) were set up in an arena (8 m long×2 m wide×4 m high) enclosed with lightweight fruit netting to prevent the pigeons from escaping. Pigeons were trained regularly (~30 min per day) for several weeks to fly between the perches (Fig. 1A). The heights of both perches were adjustable to permit control of the angle of flight. The slightly larger perch was elevated and locked into position on a 5 cm diameter PVC support pipe anchored at the ceiling and floor. The perch heights were adjusted incrementally, and the pigeons were continually encouraged to fly between them until the desired flight angle was reached (Table 2). The pigeons were conditioned to fly at each of the flight angles to be studied (60°, 30°, 0°, –30° and –60°). The actual angles of flight observed during the experiment differed slightly from the angle of the setup (see Results). For ease of discussion, however, these conditions will still be referred to as 60°, 30°, etc. The terms 'steep' and 'shallow' will be used to refer to 60°/–60° and 30°/–30° flights, respectively.

Before obtaining high-speed video recordings for 3D kinematic analysis (see below), pigeons were marked at several anatomical landmarks (Fig. 1B). These included the left and right shoulders, wrists, longest primary feather on each wing (usually the ninth), and the rump. In the global coordinate system, the *x*-axis was defined as being horizontal, in line with the perch supports; the *y*-axis was medio-lateral; and the *z*-axis was vertical.

Table 1. Morphological parameters for birds

Bird	Mass (g)	Wing length (cm)	Single wing area (cm^2)
1	416	28.5	340
2	403	29.0	354
3	522	32.3	375
4	495	26.5	338

Filming and film analysis

Three high-speed, digital video cameras (two RedLake PCI 500, RedLake Inc., San Diego, CA, USA; and one Photron FastCam-X 1280 PCI, Photron USA Inc., San Diego, CA, USA) were positioned around the flight arena. One RedLake camera was mounted on the ceiling to record dorsal views of the pigeons. The other RedLake camera was positioned near the taller perch, and the Photron camera was positioned to the side of the arena (Fig. 1A). Recordings were made at 250 frames s^{-1}, with shutter speeds of 1/500 to 1/1000 s. The flight volume from which 3D kinematics were taken (*XYZ*: 1×0.9×1 m for level flight; 1×0.9×2 m for angled flight) was calibrated using the direct linear transform method (Hatze, 1988). The calibrated volume included approximately 13% of the level flight path, 19% of the ±30° flight paths and 56% of the ±60° flight paths.

At least ten flights were recorded for each bird at each flight angle, and in general, four of these were used for analysis. Flights were selected for analysis based on the straightness of the bird's path, as viewed in the dorsal camera. The dorsal camera view was the most restricted of the three camera views, and only recordings that contained at least one full wingbeat in the dorsal camera view were used for analysis. A wingbeat was defined as the movement from one upstroke–downstroke transition to the next. At –30°, no recordings for Bird 1 met this criterion, so the results presented for –30° flight reflect only data from Birds 2, 3 and 4. Birds typically flew between the two perches using ~9 wingbeats for 0° flights, ~13 wingbeats for 30° ascents, ~11 wingbeats for –30° descents, ~11 wingbeats for 60° ascents, and ~8 wingbeats for –60° descents.

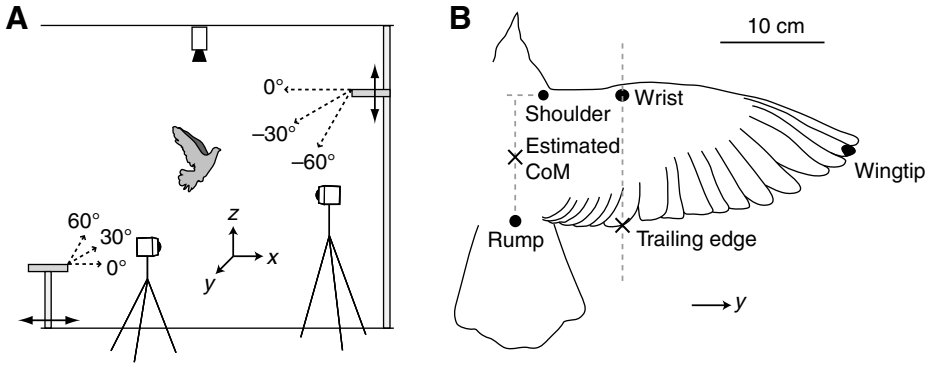

Fig. 1. (A) Experimental setup (not to scale) and (B) anatomical points measured on the bird for kinematic analysis. (A) The height of the perches and the distance between them were adjusted to encourage birds to fly at prescribed angles of ascent and descent (Table 2). Three high-speed cameras, one dorsal, one nearer to the tall perch, and one to the side of the arena, were used to record flights (*x*-axis: horizontal direction between the perches; *y*-axis: mediolateral; and *z*-axis: vertical). (B) Birds were marked at several anatomical locations. The shoulder, wrist, wingtip and rump marks were digitized, as was the point on the trailing edge of the wing, directly behind the wrist in the *x*-coordinate. The position of the center of mass (CoM) was estimated by averaging the *x*- and *z*-coordinates of the rump and shoulder and using the *y*-coordinate of the rump.

Table 2. Distances between perches and resulting flight path lengths and angles

	Vertical distance (m)	Horizontal distance (m)	Flight path length (m)	Angle (degrees)
Level flight	0.0	7.5	7.5	0
Shallow angle	2.8	5.2	5.9	28
Steep angle	3.1	1.8	3.6	60

For each flight, the wingbeat analyzed was the one that occurred closest to the middle of the dorsal camera view. This ranged from the third to the fifth-to-last wingbeat.

Kinematic marks on the birds were digitized using the custom MatLab (Version 6.5 Release 13; 2002, The MathWorks, Inc., Natick, MA, USA) program *DLTdataviewer*, written by T. Hedrick (Hedrick et al., 2004). Because the tips of the feathers on the trailing edge of the wing change position dramatically during a wingstroke, kinematic markers could not easily be used to give the angle of the wing at a particular distance along the wing. Consequently, the point on the trailing edge directly behind the wrist in the parasagittal plane was digitized. The position of the center of mass (CoM) of the bird was estimated by averaging the *x*- and *z*-coordinates of the rump and shoulders, and using the *y*-coordinate of the rump (Fig. 1B). Although the CoM of the bird's body will change during a wingbeat cycle, largely due to motion of the wings, this effect is minimal in comparison with changes in CoM position over the course of the complete wingbeat cycle. However, these time-varying inertial effects do influence accelerations during the wingbeat (Hedrick et al., 2004). Because we were observing non-maneuvering flights, we assumed that inertial effects would not create a systematic difference in mid-downstroke calculations across flight angles.

Kinematic and aerodynamic measurements

For each digitized wingbeat, the kinematic data were filtered at four times the wingbeat frequency (~30 Hz) with a low-pass fourth-order Butterworth filter implemented in a custom MatLab script. The filtered wingbeats for each bird were normalized to the same duration and then averaged within each condition. This procedure produced the standard wingbeats used for analysis. Instantaneous velocities and accelerations were calculated by numerical differentiation of the filtered positional data. Flight velocity V was calculated as the resultant of the velocities measured in each of the global x, y and z directions.

Half-stroke transitions were determined by selecting minima for the *y*-coordinate of the wingtip, i.e. when the wingtip was most medial, relative to the shoulder joint of the wing. Mid-half-stroke points were determined by selecting maxima in the *y*-coordinate of the wingtip, i.e. when the wingtip was farthest from the shoulder joint. We defined 'mid-downstroke' as the middle 16 ms (five video frames) of the downstroke. Whole wingbeats were defined as the movement from one upstroke–downstroke transition to the next.

The stroke plane was determined by performing a linear regression of the *x*- and *z*-coordinates of the kinematic data for the wingtip, relative to the shoulder, with the slope providing a measure of the stroke plane angle (Fig. 2). The maximum angle of excursion of the wing, Φ, was determined by finding the maximum angle between shoulder and paired wingtip positions in three-dimensional coordinate space.

Aerodynamic models and flight forces

The kinematics obtained in this study provided the opportunity to calculate force coefficients obtained from both the normal-forces model developed by Usherwood and Ellington (Usherwood and Ellington, 2002a) and thin-airfoil theory. Thin-airfoil theory resolves the resultant aerodynamic force on the wing into the components of lift and drag forces. Lift is defined as perpendicular to the direction of the airflow; drag as parallel to airflow (Norberg, 1990). By contrast, the normal-forces model uses the assumption that the resultant force on the wing is perpendicular to the wing itself (Usherwood and Ellington, 2002a). This force is then resolved into components that are vertical and horizontal in the global reference frame. For both models, we estimated the instantaneous resultant aerodynamic force, $F_R(t)$, by multiplying body mass by the vector sum of gravitational acceleration and instantaneous CoM acceleration. This estimate does not include the thrust necessary to overcome parasite drag, but estimates of parasite drag were all less than 0.5% of body weight. We therefore believe our estimates of $F_R(t)$ to be close to the actual value. To estimate coefficients during mid-downstroke, we averaged the values of $F_R(t)$ and the other input parameters over mid-downstroke (mds).

Because wing movement was not horizontal, the typical thin-airfoil model was modified. The usual horizontal and vertical orientations of the drag and lift forces were rotated to reflect the actual direction of wing movement (Fig. 3A), and standard formulae for lift and drag coefficients (Norberg, 1990) were modified accordingly:

$$C_{L,mds} = \frac{F_{R,mds} \cdot \sin\beta_{mds}}{\frac{1}{2}\rho \cdot A_2 \left(v_{wt,mds}\right)^2} \quad (1)$$

and

$$C_{D,mds} = \frac{F_{R,mds} \cdot \cos\beta_{mds}}{\frac{1}{2}\rho \cdot A_2 \left(v_{wt,mds}\right)^2} \ , \quad (2)$$

where $F_{R,mds}$ is the resultant force during mid-downstroke; β_{mds} is the angle between the direction of wing movement during mid-downstroke and the direction of $F_{R,mds}$; ρ is the density of air, taken

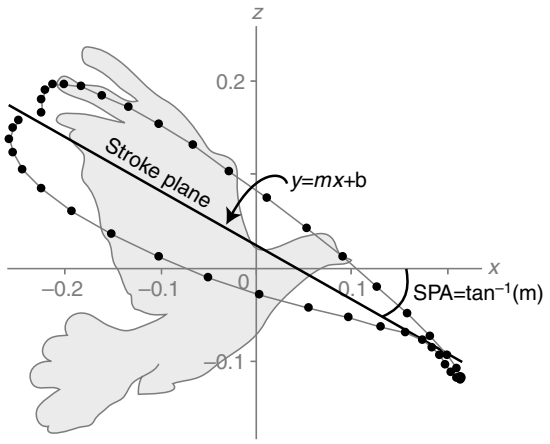

Fig. 2. The calculation of stroke plane angle (SPA). SPA is the angle corresponding to the slope of the linear regression of the *x*- and *z*-coordinates of wingtip position relative to the shoulder.

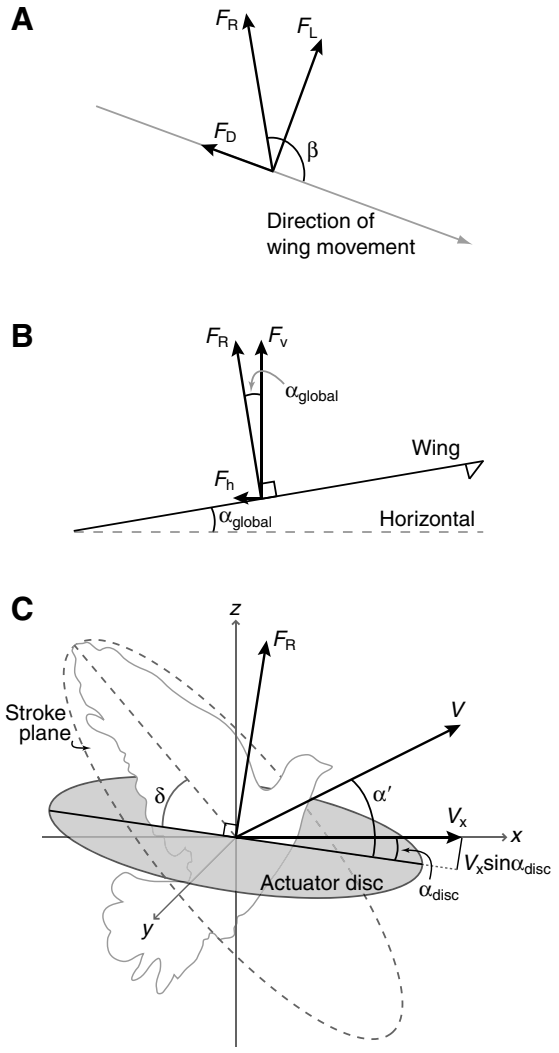

Fig. 3. The thin-airfoil model (A), the normal-forces model (B) and parameters used in calculation of P_{ind} (C). In all panels, F_R is the resultant aerodynamic force. (A) The thin-airfoil model for a wing in steady flow (e.g. Norberg, 1990), modified for non-horizontal flight. F_L is lift, and F_D is drag. β is the angle between the resultant aerodynamic force and the direction of wing movement. (B) The normal-forces model on a static wing in steady flow [after Usherwood and Ellington (Usherwood and Ellington, 2002a)]. The direction of the aerodynamic force is assumed to be normal to the surface of the wing. F_h and F_v are the horizontal and vertical forces acting on the wing, respectively. α_{global} is the angle of the wing relative to the horizontal. (C) Schematic of parameters used in calculation of P_{ind}. The area of the stroke plane is projected, using the angle δ, onto the actuator disc, which is defined as normal to F_R. α_{disc} is the angle of the actuator disc in the global reference frame. α′ is the angle between the flight velocity V and the actuator disc. As they are shown here, both α_{disc} and α′ have negative values [following Stepniewski and Keys (Stepniewski and Keys, 1984)]. V_x is the horizontal component of the flight velocity. Use of the term $V_x \sin\alpha_{disc}$ eliminates P_{PE} from the P_{ind} calculation.

to be 1.2 kg m^{-3}; A_2 is the planform area of both wings; and $v_{wt,mds}$ is the velocity of the wingtip during mid-downstroke, in the global coordinate system.

Usherwood and Ellington found that the aerodynamic force that acts on a variety of wings could be assumed to be normal to the wing (Usherwood and Ellington, 2002b). Resolving the aerodynamic force into global vertical and horizontal components gives a clearer idea how much force is providing weight support and how much force is resisting horizontal forward motion of the wing (Fig. 3B). Calculating the vertical force coefficient C_v required measuring chordwise strips of the wing. Each bird's wings were photographed and digitally divided into 14 chordwise sections using Adobe Photoshop CS (Version 8.0; 2003, Adobe Systems Incorporated, San Jose, CA, USA). The width, length, and area of each section were measured using Scion Image (Release Beta 4.0.2; 2000 Scion Corporation, Frederick, MD, USA). The CoM velocity was incorporated into the equations for the normal-forces model (Usherwood and Ellington, 2002a):

$$C_{v,mds} = \frac{F_{v,mds}}{\frac{1}{2}\rho \cdot 2 \cdot \sum_{i=1}^{i=I} A_i \left(\omega_{mds} \cdot r_i + V_{mds}\right)^2}, \quad (3)$$

where $F_{v,mds}$ is the vertical component of force (including body weight) during mid-downstroke; i is the number of the wing strip; I is the total number of chordwise strips; A_i is the planform area of the ith wing strip; ω_{mds} is the angular velocity of the wing during mid-downstroke; r_i is the distance of strip i from the shoulder; and V_{mds} is the CoM velocity during mid-downstroke. The horizontal force coefficient C_h was then calculated as:

$$C_h = C_v \cdot \tan(\alpha_{global}), \quad (4)$$

where α_{global} is the angle of the wing relative to the horizontal, in the global reference frame.

Angle of attack (AoA) was calculated as the angle between the wing chord at the wrist, and the resultant velocity of: the velocity at the wrist, relative to the shoulder, and the CoM velocity. Tobalske et al. included the vertical component of induced velocity when calculating AoA (Tobalske et al., 2007). We did not follow their approach, though doing so for the data presented here would decrease the calculated value of AoA by ~10°.

Energy changes and power calculations

Potential energy change (ΔPE, or ΔPE per cycle) was calculated from the weight of the bird and the change in CoM vertical position over the course of the wingbeat. 'PE flight power' (P_{PE}) was calculated by dividing ΔPE by the duration of the wingbeat, $\Delta t_{wingbeat}$.

To estimate aerodynamic power over the course of a wingbeat, we adapted the approaches of Wakeling and Ellington (Wakeling and Ellington, 1997a; Wakeling and Ellington, 1997b) and Askew et al. (Askew et al., 2001) to angled flight (Fig. 3C). Induced velocity w was calculated using the general formula for a rotor traveling at velocity V, at an angle α′ to the actuator disc:

$$w^4 - 2Vw^3 \sin\alpha' + V^2 w^2 - \left(\frac{F_R}{2\rho A_{disc}}\right)^2 = 0, \quad (5)$$

where A_{disc} is the area of the actuator disc (Stepniewski and Keys, 1984). F_R is the resultant aerodynamic force for the wingbeat, calculated as the product of the mass and the vector sum of gravitational acceleration and the bird's overall acceleration that occurred during the wingbeat. Overall acceleration was calculated as the difference between the mean velocity of the final 12 ms and the mean velocity of the first 12 ms of the wingbeat cycle. Following Stepniewski and Keys (Stepniewski and Keys, 1984), the angle α′ has a negative value when the disc is tilted below the velocity vector (as in Fig. 3C). Because the stroke plane was not necessarily normal to F_R, A_{disc} was calculated as in Ellington (Ellington, 1984):

$$A_{disc} = \Phi R^2 \cos\delta, \quad (6)$$

where Φ is the angle of excursion (described above), R is the length of the wing, and δ is the angle between the stroke plane and actuator disc. Induced power is the product of F_R and the axial velocity, which is the velocity of air through the actuator disc:

$$P_{ind} = F_R(k_{ind}w - V\sin\alpha') , \quad (7)$$

where P_{ind} is induced power and k_{ind} is a correction factor for induced velocity. However, Askew et al. (Askew et al., 2001) point out that this calculation of induced power includes the rates of change of potential energy and kinetic energy. We therefore eliminated those terms from the formulation of P_{ind} and calculated it as:

$$P_{ind} = F_R k_{ind} w - mgV_x\sin\alpha_{disc} , \quad (8)$$

where k_{ind} is taken to be 1.2 (Pennycuick, 1975). The induced velocity term, $F_R k_{ind} w$, remains unchanged when kinetic and potential energy change are excluded. To eliminate the potential energy change from the forward velocity term ($V\sin\alpha'$ in Eqn 7), we used only the horizontal component of flight velocity, V_x. The term $V_x\sin\alpha_{disc}$ gives the axial component of V_x, when α_{disc} is the angle of the actuator disc in the global frame. As with α', α_{disc} has a negative value when the disc is tilted below the global horizontal (as in Fig. 3C). To eliminate the kinetic energy change, we did not include acceleration in multiplying the forward velocity term, hence the use of mg instead of F_R in the right-hand term of Eqn 8.

Following Rayner's observation (Rayner, 1999) that previous estimates of parasite drag, such as those of Pennycuick on pigeons (Pennycuick, 1968b), were about three times too high, we assumed a value of 0.15 for the parasite drag coefficient for the body, $C_{D,par}$. We then estimated parasite power, P_{par} as:

$$P_{par} = 0.5\rho A_{fron} C_{D,par} V^3 , \quad (9)$$

where A_{fron} is the frontal area of the bird's body and tail. Calculating parasite drag required knowing the frontal area of the bird at different angles. One pigeon (Bird 4) was photographed while being held at angles from 90° to –60° at 30° increments. A ruler was vertically positioned next to the bird for calibration. Using Scion Image, the outline of the bird was traced and the frontal area calculated for each angle. A sine curve was fit to the data, which allowed estimation of frontal area at any angle.

As suggested in Rayner (Rayner, 1979) we used a value of 0.02 for the profile drag coefficient, $C_{D,pro}$, similar to Askew et al. (Askew et al., 2001). We estimated profile power, P_{pro} as:

$$P_{pro} = 2\sum 0.5\rho \cdot C_{D,pro}\left[\left(\omega \cdot r_i\right)^3 \cdot A_i\right] . \quad (10)$$

Total power, P_{tot}, is the sum of CoM PE and KE power, and the components of aerodynamic power:

$$P_{tot} = P_{PE} + P_{KE} + P_{ind} + P_{par} + P_{pro} . \quad (11)$$

To address our hypothesis that $P_{tot}=P_{tot,lev}+P_{PE}$, and because 'level' flights were not strictly level (see Results), for each bird we subtracted the value of P_{PE} for level flight from P_{tot} for level flight:

$$P_{lev} = P_{tot,lev} - P_{PE,lev}, \quad (12)$$

and added the values of P_{PE} observed for each bird's angled flights to the value of P_{lev} for that bird. This reformulates our hypothesis as:

$$P_{tot} = P_{lev} + P_{PE} . \quad (13)$$

Statistical analysis

For statistical analysis, flight angles were grouped into categories of '–60', '–30', '0', '30' and '60'. All statistical tests were performed in Systat (Version 10.2; 2002; Systat Software, Inc., San Jose, CA, USA). Because Bird 1 did not perform –30° flights suitable for analysis, repeated-measures analyses excluded data for –30° flights. For the same reason, multiple paired t-tests had two degrees of freedom when comparing 30° flights with other conditions, and three degrees of freedom otherwise. The sequential Bonferroni method (Rice, 1989) was used to determine significance of comparisons between each pair of conditions. Linear regressions were performed on all standard wingbeats for all conditions.

RESULTS

Variation among individuals was not significant for any of the data presented here. In the figures, lines connect means of values at each condition, and asterisks denote significant differences, as determined by repeated-measures analyses. Values are reported as mean ± s.e.m. Representative flights (all from Bird 3) are included as Movies 1–5 in supplementary material.

Kinematics and flight speed

Actual angles of flight were generally close to the angle of the setup (Fig. 4A, Fig. 5B). The 60° ascending flights averaged a vertical flight angle of 60±1°, and 30° ascents averaged 27±1°. Level flights showed a slight negative flight angle, –4±1°, because the birds tended to jump upward when taking off, and then descend gradually as they approached the opposite perch. The –30° descents averaged –29±1°, and –60° descents averaged –53±1°. Vertical distances traveled during the standard wingbeat were not significantly different between 30° and 60° flights (0.30±0.02 m and 0.23±0.04 m, respectively; P=0.35), nor between –30° and –60° flights (–0.35±0.04 m and –0.35±0.02 m, respectively; P=0.16). Horizontal distances traveled during the standard wingbeats for 30°, 0°, and –30° flights did not differ significantly from each other (0.48±0.05 m, 0.64±0.03 m and 0.61±0.03 m, respectively; $P\geqslant 0.019$ for each comparison). Horizontal distance traveled for 60° flights was significantly less than all other conditions (0.18±0.01 m; $P\leqslant 0.007$ for each comparison) and that for –60° flights was significantly less than that for 0° and –30° flights (0.26±0.01 m; P=0.001 and P=0.010, respectively).

Flight speed ranged from 2.7 to 5.0 m s^{-1} and varied significantly across the four birds over the range of vertical flight angles studied (repeated-measures ANOVA, $P<0.001$, F=31.457; Fig. 4B). Flight speed averaged 3.6±0.2 m s^{-1} for –60° flight and increased to an average of 4.9±0.1 m s^{-1} for –30° flight, which showed the greatest flight speed for all conditions. Flight speed decreased with increasing flight angle to 2.9±0.1 m s^{-1} for 60° ascent. The vertical component of flight velocity ('vertical flight velocity', Fig. 4B) showed the steepest increase from shallow descent to shallow ascent, increasing from –2.4±0.1 m s^{-1} at –30° to 1.8±0.1 m s^{-1} at 30°. Vertical flight velocity for –60° descent was –2.9±0.2 m s^{-1} and was not significantly different from that at –30° (P=0.11).

Wingbeat frequency (WBF) ranged from 6.1 to 9.6 Hz over all standard wingbeats analyzed (Fig. 4C). Differences in WBF values among conditions tended toward varying significantly among flight angles (repeated-measures ANOVA, P=0.053, F=3.766) and, with a larger sample size, this may well have been borne out. WBF was more variable among birds for ascending flights. Angles of wing excursion, as measured from the shoulder to the wingtip, also did not vary significantly across flight angles (repeated-measures ANOVA, P=0.317, F=1.356). Shoulder–wingtip angles of excursion were quite large, reaching a maximum of 228° for Bird 2 during –60° flight. Angles of wing excursion measured from shoulder to wrist were more modest, but still reached a maximum of 153° (Bird

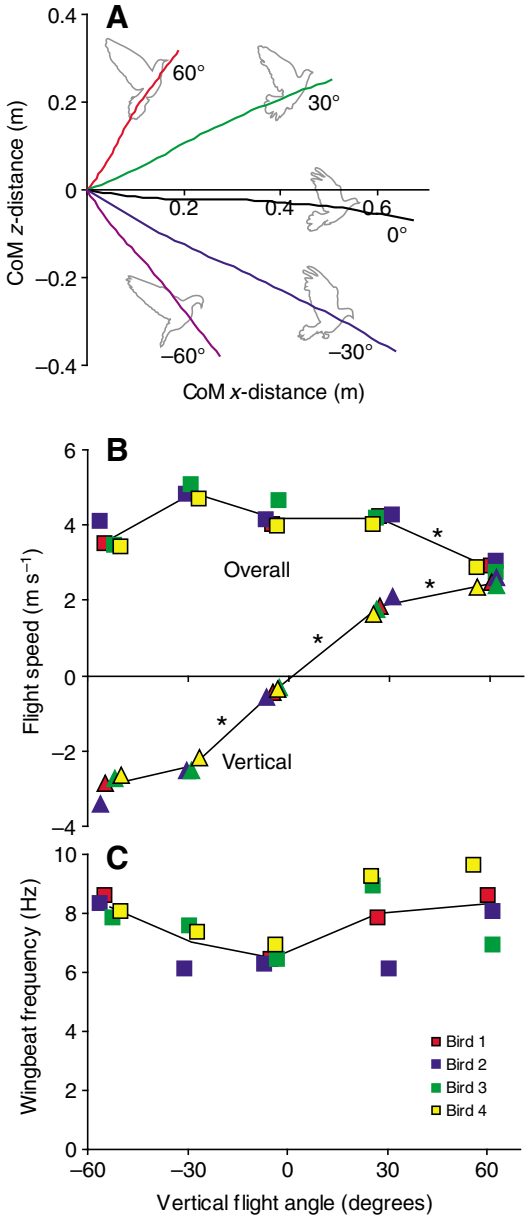

Fig. 4. (A) Observed flight paths of the four birds, (B) average overall and vertical flight speeds during the digitized wingbeat and (C) wingbeat frequency *versus* vertical flight angle. (A) Average paths traveled by the pigeons for each flight angle during one wingbeat, with starting position normalized to the origin. Vertical distances traveled were similar between 30° and 60° flights, and also between –30° and –60° flights. Birds traveled greater horizontal distances for ±30° and 0° flights than for ±60° flights. (B) Overall flight speed (squares) showed an increase from –60° to reach a maximum at –30°. Speed decreased from –30° descent to 60° ascent. The vertical component of flight velocity (triangles) showed the greatest differences between ±30° and 0° flights, and was not significantly different between –30° and –60° descents (P=0.11). (C) Wingbeat frequency (WBF) ranged from 6.1 Hz to 9.6 Hz with greater variability observed among individuals for ascending flight. WBF did not differ significantly across vertical flight angles (P=0.053, F=3.77). In B and C, as well as in subsequent figures, each point is the data for a standard wingbeat, lines connect means of adjacent flight angles, and asterisks indicate significant differences. Data for individual birds are color-coded.

1 at 30°). The angular velocity of the wing at mid-downstroke showed a pattern similar to WBF, reflecting the similarity of wing excursion angles across flight angles.

Wingstroke paths are illustrated in Fig. 5B,C. For both steep ascent and steep descent, the wingtip always remained craniad to the wrist, indicating that the wing was held in a more protracted position. In level flight, the path of the wingtip entirely included the path of the wrist (in lateral view). During shallow ascent and shallow descent, the pattern of wingtip and wrist paths was intermediate. The kinematic pattern in the lateral view thus appears symmetric, as the wing is more protracted for steeper flights, whether ascending or descending. The paths of the wingtip and wrist in dorsal view showed little variation across flight angles, except for somewhat greater stroke amplitudes for 30°, 60° and –60° flights, relative to level flight.

Potential energy change and *PE* flight power

For ascending flight trials at 30° and 60°, the potential energy change over a full wingbeat cycle ('ΔPE per cycle', Fig. 6A) averaged 1.1±0.1 J and 1.4±0.1 J, respectively, but did not differ significantly (P=0.17). For –30° and –60° descent trials, ΔPE per cycle was again similar (P=0.32), averaging –1.6±0.1 J for both. As noted above, level flight trials were slightly negative (–0.28±0.03 J) due to the slight descent the birds used for the 0° perch setup.

Because wingbeat frequency (Fig. 4C) and hence cycle duration, did not show a strong pattern of variation across flight angles, *PE* flight power (Fig. 6B, P_{PE}) showed a pattern similar to ΔPE. Ascending flights at 30° and 60° averaged *PE* flight powers of 8.2±0.3 W and 11.0±0.5 W, respectively, which were significantly greater than P_{PE} for level flight (–1.8±0.2 W; P<0.001 for both comparisons) and significantly different from each other (P=0.002). P_{PE} of descending flights at –30° and –60° averaged –11.1±0.9 W and –13.0±0.5 W respectively, and were not significantly different from each other (P=0.75). Regression of *PE* flight power against flight angle showed a slope of 0.234 W deg.$^{-1}$, which was significantly different from zero (r^2=0.95, P<0.001).

Aerodynamics, aerodynamic power and force

Wing stroke plane angle relative to the horizontal (SPA; Fig. 5A, Fig. 7A) did not differ significantly among flight angles. Though the difference was not significant, shallow and level flights showed somewhat steeper SPAs than did steep flights. Body angle in the global frame was steepest for 60° ascent and most horizontal at –30° flights, with –60° flight showing a mean body angle intermediate to level and shallow ascent (Fig. 5A). Body angle showed significant variation overall (repeated-measures ANOVA, P=0.004, F=9.353), but *post hoc* paired *t*-tests were all non-significant with the Bonferroni correction ($P \geqslant 0.014$ for each comparison). The stroke plane angle relative to the body angle (Fig. 5A) was greatest for 60° ascent and decreased with decreasing flight angle, with a minimum at –30°.

Angle of attack at mid-downstroke (AoA) was greatest for steep descending flight (68±3°, Fig. 7B). AoA decreased as flight angle increased to –30°, 0° and 30° (AoA=47±1°, 40±1° and 35±2°, respectively). AoA increased slightly as flight angle increased to 60° flight (AoA=41±3°). Differences in AoA between –60° and 0°, 30° and 60° tended toward significance (P=0.0054, 0.006 and 0.007, respectively), but following the sequential Bonferroni method, they were not deemed statistically significant.

The power calculations for the different vertical flight angles are shown in Fig. 8. Total power (P_{tot}) estimates ranged between –5.13 and 26.2 W and varied significantly across flight angles (repeated-measures ANOVA, P=0.001, F=15.381). Induced power (P_{ind}) calculations ranged between 3.5 and 24.6 W, and on average were greater for descending flights. P_{ind} also varied significantly across

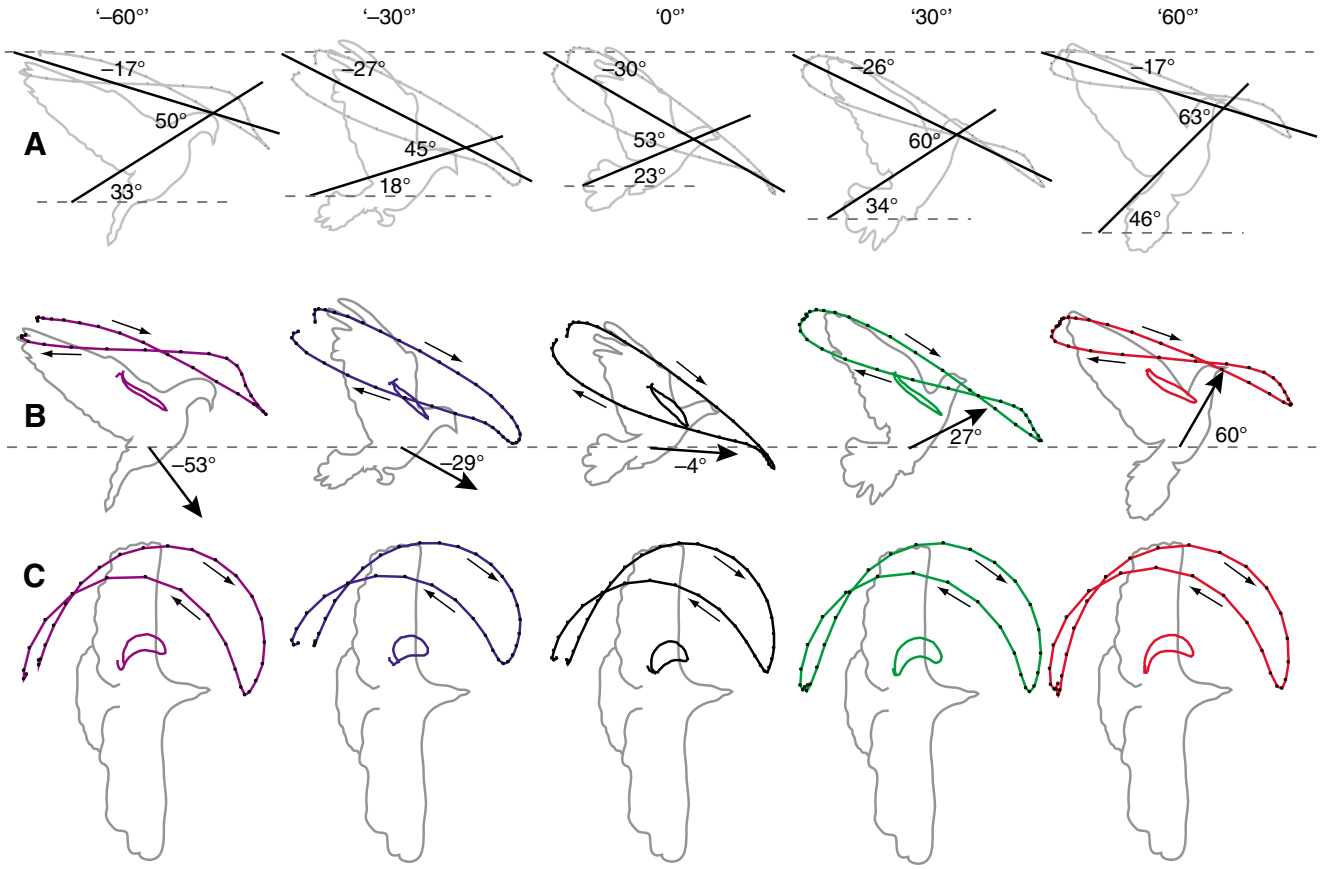

Fig. 5. Illustration of flight kinematics for each flight condition. Gray broken lines represent the horizontal. (A) From top down: stroke plane angle relative to the horizontal, stroke plane angle relative to body angle, and body angle for each condition. The body angle lines do not exactly correspond to the bird outlines because the outlines were made from actual (non-averaged) images from oblique camera views. (B) Lateral views of wingtip and wrist kinematics and mean observed flight angle for the setup condition. The wingtip path is more craniad for steeper flights. (C) Dorsal view of the wingtip and wrist kinematics. Mid-downstroke posture varied little across conditions, and the outline for level flight is shown for all.

flight angles (repeated-measures ANOVA, P=0.006, F=8.450). Power due to changes in kinetic energy varied between 4.2 and –6.6 W, but did not vary significantly from zero (P=0.239) or across flight angles (repeated-measures ANOVA, P=0.438, F=0.995). Parasite power averaged less than 0.09±0.01 W for all conditions, and profile power averaged less than 0.67±0.09 W for all conditions. Because of their small magnitudes relative to P_{tot}, parasite and profile powers are not shown in Fig. 8A. Differences between P_{tot} and P_{lev}+P_{PE} were not significant for any of the flight angles (paired t-tests, P=0.134 for –60° and $P \geqslant 0.411$ for all other conditions).

Across flight angles, the magnitude of F_R averaged between 4.18 and 5.20 N, and was similar to the bird's weight ($P \geqslant 0.108$; Table 3). F_R magnitude was somewhat greater for descending flights. The variation in F_R across flight angles was significant overall but not among conditions (repeated-measures ANOVA, P=0.028, F=4.899; paired t-tests, $P \geqslant 0.028$ for each comparison). Moreover, F_R orientation was similar to the vertical ($P \geqslant 0.465$ for all conditions) and did not vary significantly across flight angles (repeated-measures ANOVA, P=0.861, F=0.247). The force coefficients C_v, C_h and C_L did not show significant variation among conditions (repeated-measures ANOVA, C_v: P=0.137, F=2.387; C_h: P=0.156, F=2.213; C_L: P=0.159, F=2.188). Marginally significant variation for C_D was observed overall (repeated-measures ANOVA, P=0.043, F=4.106), but *post hoc* paired t-tests were all non-significant ($P \geqslant 0.083$ for each test). The calculated values of these coefficients are shown in Table 3.

DISCUSSION

In this study, we sought to determine whether the power necessary for a bird to fly at an angle could be estimated as the simple sum of the total power required for level flight (P_{lev}) and the power necessary for the center of mass change in potential energy (P_{PE}). We found that this was generally the case. The sum of P_{lev} and P_{PE} for each angle was not significantly different from the total power (P_{tot}) for any ascending or descending flight angle, though the difference was greatest for –60° flight (Fig. 8B). This larger difference was due to the increased induced power requirement calculated for steep descent (Fig. 8A). That P_{tot} and P_{lev}+P_{PE} were similar implies that pigeons generally do not balance the power lost or gained through potential energy change by a corresponding increase or decrease in kinetic energy (P_{KE}) or induced power (P_{ind}). Thus, as expected, ascending flight requires more power than level flight, and descending flight requires less power than level flight. As noted, however, during –60° flight the birds' deceleration and slower flight velocity led to an increased induced power requirement, resulting in a higher P_{tot} and an increased difference between P_{tot} and P_{lev}+P_{PE} for steep descent.

The average total power estimated in this study for level flight (7.96±3.09 W) was not dissimilar to that found by Pennycuick

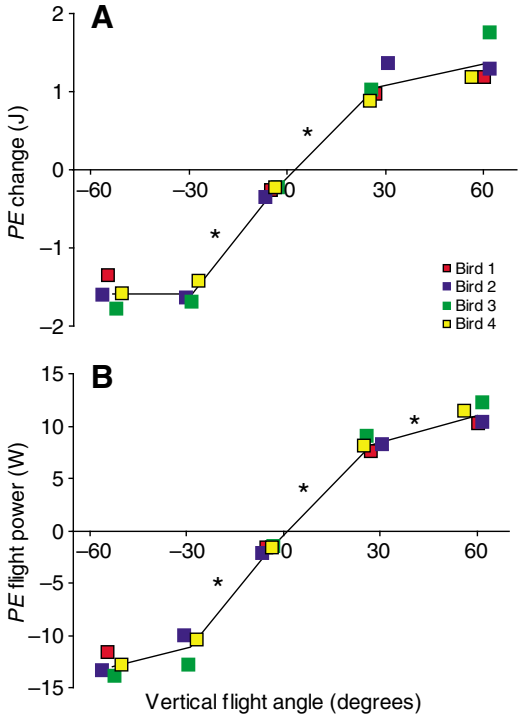

Fig. 6. (A) Center of mass (CoM) potential energy change (ΔPE) per wingbeat, and (B) CoM *PE* flight power ($\Delta PE/\Delta t_{wingbeat}$) *versus* vertical flight angle. ΔPE/wingbeat cycle values were similar for ascending flight angles (means for 60°=1.41±0.14 J; 30°=1.10±0.11 J), and also similar for descending flight angles (means for –60°=–1.55±0.09 J; –30°=–1.53±0.08 J). *PE* flight power values were significantly different among all flight angles except between steep and shallow descent (P=0.073 for –60° *vs* –30°; $P \leqslant 0.012$ for all other comparisons).

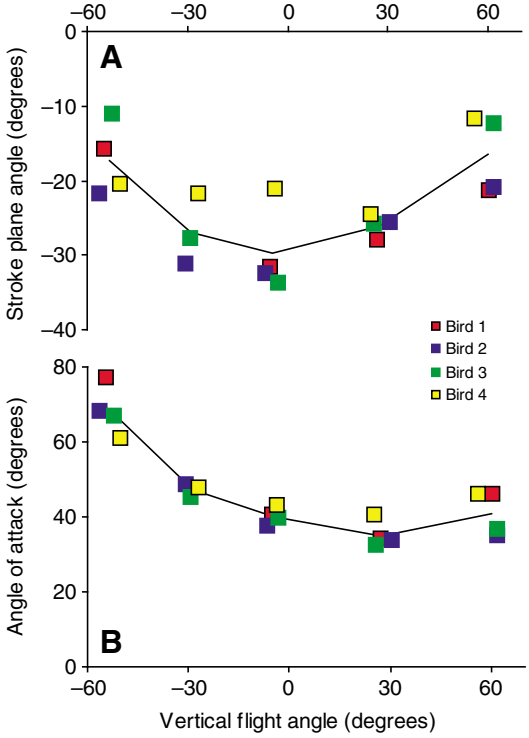

Fig. 7. (A) Stroke plane angle (SPA) relative to horizontal and (B) angle of attack (AoA) at mid-downstroke *versus* flight angle. SPA was more inclined for level and shallow ascent and descent, and more horizontal for steep ascent and descent. Values of AoA decreased from steep descent through shallow ascent, and then increased slightly from shallow to steep ascent.

(Pennycuick, 1968a) for pigeons in level flight at corresponding speeds (~9.5 W). However, calculation of aerodynamic power using differential pressure measurements on the wings of pigeons of similar mass (Usherwood et al., 2005) gave a value of 26 W during level flight, considerably higher than the value calculated here. Actual power output by the pigeons is likely to have been higher than the estimates of power presented here because the calculation of induced power assumes an ideal momentum jet with small tip losses (k=1.2). Calculations of induced power are thus minimum values for what may be expected in comparison to prior measurements of aerodynamic power (Usherwood et al., 2005) and muscle mechanical power (Biewener et al., 1998; Soman et al., 2005) of pigeons during flight.

The ΔPE per wingbeat cycle showed an interesting pattern between shallow and steep flights. For both ascending and descending flights, there was little difference in the ΔPE per cycle for shallow *versus* steep flight, suggesting that the birds were limited in the potential energy they could gain or dissipate during a single wingbeat cycle. This result, in addition to the data showing shorter horizontal distances traveled during steeper flight (Fig. 4A), indicates that in order to fly at steeper angles, the pigeons primarily regulated the forward distance traveled per wingbeat.

Despite the large range of flight angles and the large changes in *PE* that this required of the birds during flight, F_R was always similar to the vertical and had a magnitude similar to the bird's weight. Although perhaps counterintuitive, this result is not unexpected, as the dominant force a bird must overcome while flying at low speeds is its weight, regardless of its flight direction. Because the difference in aerodynamic force necessary to maintain steady slow flight at even extremely different angles of ascent or descent is small, the kinematic differences underlying the production of aerodynamic force are also likely to be small. Such differences, therefore, may be difficult to distinguish, even when employing the 3D kinematics methods used here to evaluate flight performance. This likely explains why we often did not observe distinct kinematic patterns that varied with flight angle.

Nevertheless, we did see trends in the data relative to flight angle. As expected, angle of attack (AoA) was highest for descending flight (Fig. 7B). But contrary to our expectations, AoA did not decrease from level to ascending flights. This indicates that for ascending flight the birds altered the angle of their wings and wing movement (stroke plane angle) in such a way that the wing angle did not change relative to the resultant angle of the CoM velocity and the wrist velocity relative to the shoulder. Overall, AoA was quite high, averaging 46° across all standard wingbeats and reaching 77° for Bird 1 at –60°. Because of the high values of AoA, the thin-airfoil model may not be applicable here, even as modified for this study, as it assumes a thin airfoil with modest AoA.

Speed and kinematic implications for aerodynamic mechanisms

Flight speed was not constant across flight angles. Steep ascending flights were the slowest, suggesting that the energy expended by the bird was directed more toward increasing its CoM potential energy than flying more quickly. Though the differences were not

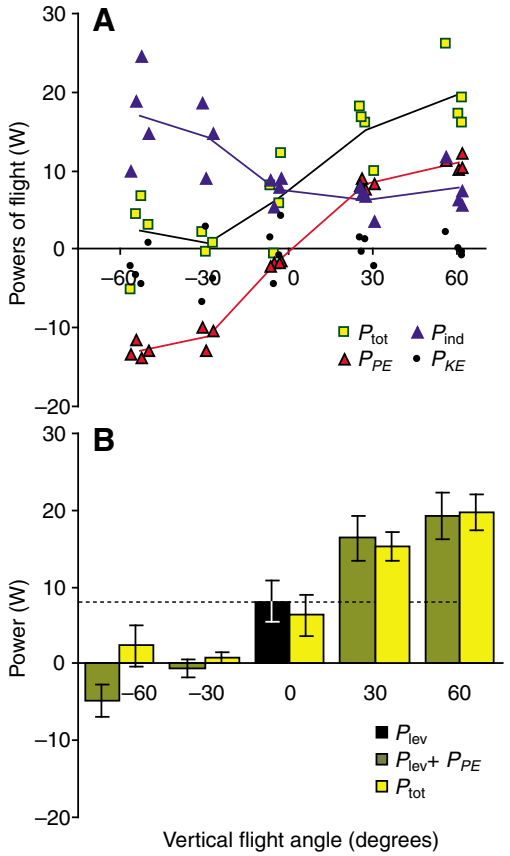

Fig. 8. Powers of flight *versus* flight angle. (A) P_{tot}, P_{PE}, P_{ind} and P_{KE}. P_{tot} is the sum of P_{PE}, P_{ind}, P_{par}, P_{pro} and P_{KE}. Because of the relatively small magnitudes of P_{par} and P_{pro}, they are not shown on the figure. P_{PE} is the same as shown in Fig. 6B. The slope of the regression of P_{KE} *versus* flight angle did not differ from zero (P=0.11). (B) Estimated P_{tot} for all conditions, and the value of $P_{lev}+P_{PE}$ for ascending and descending conditions, with standard error bars. The broken line indicates the value of P_{lev}, which is the value of P_{tot} for level flight without the P_{PE} for level flight. For every non-level flight condition, P_{tot} and $P_{lev}+P_{PE}$ were similar (paired *t*-tests, P=0.134 for –60° and $P \geqslant 0.411$ for all other conditions).

statistically significant, on average the fastest flights were observed for shallow descent, which was also the flight angle for which P_{tot} was lowest (Fig. 8B). This suggests that the birds may take advantage of gravity to reach the lower perch. However, during the steepest descent angle (–60°) studied, the birds decelerated and flew more slowly, reflecting an attempt to maintain control along a flight path that was essentially a steeply angled fall.

Wingbeat frequency (WBF) varied, but was not significantly different across flight angles, indicating that faster wingbeats may not be necessary for inclined flight as we had expected. However, a larger sample size may have borne out a significant increase in WBF across flight conditions, with the greatest WBF occurring at the steepest flight descents and ascents (Fig. 4C).

Stroke plane angle (SPA) also varied, but not significantly across vertical flight angles. SPA was somewhat more horizontal at steep flight angles, suggesting the pigeons may have forced more air downward. For steep ascending flight, this could assist in upward propulsion; for steep descending flight, it could serve to slow the bird and give it more control. In the bumblebee *Bombus terrestris* (Dudley and Ellington, 1990), and three bird species (Tobalske and Dial, 1996; Tobalske et al., 2007), SPA was found to be more horizontal for slower flight, when forcing more air downward may assist with weight support. Steep ascent and descent were the conditions for which the slowest flights were observed, so the more horizontal orientation of the stroke plane may be due in part to the low flight speed.

For level flight, wingstroke kinematics (Fig. 5B,C) were similar to those depicted in Tobalske and Dial (Tobalske and Dial, 1996) for pigeons in level flight at 8 m s^{-1}. In level flight, the path of the wingtip, viewed laterally, surrounded the entire path of the wrist. As flight became progressively steeper, for both ascent and descent, the wingtip path was more craniad, indicating that the pigeons used a more protracted wing position throughout the wingstroke for steep vertical flight angles. Tobalske and Dial (Tobalske and Dial, 1996) observed that as flight speed increased in pigeons, the wingtip path became more caudad. The kinematics seen here may reflect a continuation of this trend to lower speeds. The slowest flights observed in this study were during steep ascent and descent, which were also the conditions that showed the most craniad position of the wingtip path.

Flight at steeper angles

The present study examined flight at vertical angles from –60° to 60°, at 30° increments. Dial and Biewener (Dial and Biewener, 1993) studied muscle function in smaller wild-type pigeons during a variety of flight modes, including 90° vertical ascent and near-vertical (~–80°) descent. During vertical ascent, they observed the highest wingbeat frequencies, averaging 9.1±0.3 Hz. This value fits within the range observed here for 60° ascent (6.9–9.6 Hz), but is somewhat higher than the average at this flight angle (8.3±0.6 Hz). In near-vertical descent, Dial and Biewener (Dial and Biewener, 1993) found that WBF averaged 8.8±0.5 Hz, which is above the range for –60° flight observed here (7.8–8.6 Hz). Once again, this suggests that, although the variation in WBF among flight angles was not significant here, there may be an overall trend of increasing WBF with increasing steepness of flight ascent and descent, though differences in body mass of the pigeons used in the two studies may also affect this pattern.

The data presented here for flight speed in pigeons can also be extended using data from Dial and Biewener (Dial and Biewener, 1993). For 60° ascent, average flight velocity was 2.9±0.1 m s^{-1}.

Table 3. F_R and force coefficient values

	Flight angle (degrees)				
	–60	–30	0	30	60
F_R (N)	4.45±0.25	4.41±0.33	4.18±0.29	5.20±0.20	5.13±0.41
C_L	1.18±0.16	1.72±0.10	1.44±0.29	0.77±0.13	0.74±0.20
C_D	1.15±0.21	1.07±0.41	1.01±0.08	0.44±0.19	0.67±0.06
C_v	2.65±0.26	2.51±0.19	2.50±0.25	1.51±0.35	2.09±0.30
C_h	1.46±0.32	0.50±0.10	0.97±0.25	0.81±0.22	1.74±0.25

During vertical ascent, Dial and Biewener found that the average speed was 2.6 m s^{-1}. This suggests that flight speed decreases further for ascent angles beyond 60°. However, this difference between 60° and 90° ascent (0.25 m s^{-1}) is not as great as the difference between shallow and steep ascent (1.29 m s^{-1}), so flight speed may begin to be constrained at an angle below 60°.

Future directions

Although we did not explore the contributions of the tail to aerodynamic forces produced by the pigeons in this study, preliminary data suggest that tail spread may vary approximately 30° and tail angle relative to the body approximately 20° across the conditions we examined here. Future analysis of these contributions during different modes of flight would, therefore, be interesting to explore in more detail.

An understanding of ascending and descending flight would also be enhanced by comparing how changes in flight velocity affect the kinematics and power requirements of flight at different flight angles. Some of the kinematic observations made here for 60° ascents and descents, such as steeper stroke plane and more protracted wing position, may be due in part to the slow speeds the pigeons used for steep flight. Analysis of faster flights might clarify the role of these factors in ascending and descending flight. The use of a larger flight arena may allow birds to select preferred flight speeds for different flight angles, which may lower their aerodynamic power requirement.

The methods we used to estimate aerodynamic power requirements were based on kinematic data and aerodynamic theory, which required the estimation of force coefficients as well as assumptions about the forces acting on the wings and bird. The application of other methods for calculating aerodynamic power to the situations of ascending and descending flight, and the comparison of such results with those presented here, would help determine the validity of the methods used here. Differential pressure sensors would provide data from which the forces on the wing could be calculated (Usherwood et al., 2005). *In vivo* muscle data would allow measurement of mechanical power output of the flight muscles (Dial and Biewener, 1993; Biewener et al., 1998; Soman et al., 2005). These other methods may be particularly useful in understanding the aerodynamic forces and power requirements in steep descending flight, where the greatest difference between P_{tot} and $P_{lev}+P_{PE}$ was observed. Analysis of multiple wingbeats along an inclined flight path might also provide better calculations of aerodynamic power; however, this must be traded-off against kinematic resolution of individual wingbeats, which was our focus here.

Nevertheless, our results show that, once pigeons achieve a steady flight path across a large range of ascent and descent angles at relatively slow speed, the primary force that must be produced is to support their weight. It could be that the initiation of or transition to ascending or descending flight, particularly at higher speeds, would exhibit larger changes in resultant aerodynamic force magnitude and direction. An examination of how birds initiate changes in flight angle, or maneuver to fly above or below an obstacle, is likely to clarify how flight kinematics and forces are adjusted to execute these flight behaviors.

While wild rock pigeons are cliff-dwellers and likely to be well-adapted to ascending and descending flight, some species, such as aerial predators, are likely more specialized for fast ascent and descent. Determining what morphological traits make a species a faster flier at steep vertical angles, such as wing shape and sweep angle, wing loading or muscle morphology, would also likely provide further insight into the aerodynamics and biomechanics of ascending and descending flapping flight.

LIST OF SYMBOLS AND ABBREVIATIONS

a_z	vertical component of whole-body acceleration
A_2	area of both wings
A_{disc}	area of actuator disc
A_{fron}	frontal area of bird
A_i	area of *i*th wing section
AoA	angle of attack
CoM	center of mass
c_r	wing chord at distance *r*
C_D	coefficient of drag
$C_{D,par}$	coefficient of parasite drag for the body
$C_{D,pro}$	coefficient of profile drag
C_h	horizontal force coefficient
C_L	coefficient of lift
C_v	vertical force coefficient
F_D	drag force (force parallel to direction of wing movement)
F_h	horizontal component of resultant aerodynamic force
F_L	lift force (force normal to direction of wing movement)
F_R	resultant force magnitude
F_v	mass * vertical acceleration
F_x	mass * horizontal (forward) acceleration
$\boldsymbol{g}$	gravitational acceleration
i	index for wing section
I	number of wing sections
k_{ind}	induced velocity correction factor
m	mass
P_{aero}	aerodynamic power
P_{ind}	induced power
P_{KE}	power due to change in kinetic energy
P_{lev}	power for level flight, excluding potential energy change
P_{par}	parasite power
P_{PE}	power due to change in potential energy
P_{pro}	profile power
P_{tot}	total power
$P_{tot,lev}$	total power for level flight
r	distance on wing from shoulder
r_i	distance of wing section from shoulder
R	length of wing
SPA	stroke plane angle
t	time
v_{wt}	global velocity of the wingtip
V	flight velocity
$V(t)$	instantaneous velocity
V_x	horizontal component of flight velocity
w	induced velocity
WBF	wingbeat frequency
α'	angle between the flight velocity and the actuator disc
α_{disc}	angle of the actuator disc, in the global reference frame
α_{global}	angle of the wing, in the global reference frame
β	angle between direction of force and direction of wing movement
δ	angle between the stroke plane and the actuator disc
ρ	density of air
ω	angular velocity of wing
ΔKE	change in kinetic energy
ΔPE	change in potential energy
$\Delta t_{wingbeat}$	wingbeat duration
Φ	angle of excursion
Subscripts:	
lev	level flight
mds	mid-downstroke

We would like to thank Pedro Ramirez for caring for the pigeons, and the many people at the Concord Field Station who assisted in the experiments. We greatly appreciate the expert guidance that Jim Usherwood provided in the early stages of data analysis. We are also grateful to Ty Hedrick and Bret Tobalske for their expert guidance and for helpful comments on earlier versions of this paper, as well as the critical advice offered by two referees.

REFERENCES

Altshuler, D. L., Dudley, R. and McGuire, J. A. (2004). Resolution of a paradox: hummingbird flight at high elevation does not come without a cost. *Proc. Natl. Acad. Sci. USA* **101**, 17731-17736.

Askew, G. N., Marsh, R. L. and Ellington, C. P. (2001). The mechanical power output of the flight muscles of blue-breasted quail (*Coturnix chinensis*) during take-off. *J. Exp. Biol.* **204**, 3601-3619.

Biewener, A. A., Corning, W. R. and Tobalske, B. T. (1998). *In vivo* pectoralis muscle force–length behavior during level flight in pigeons (*Columba livia*). *J. Exp. Biol.* **201**, 3293-3307.

Bundle, M. W. and Dial, K. P. (2003). Mechanics of wing-assisted incline running (WAIR). *J. Exp. Biol.* **206**, 4553-4564.

Bundle, M. W., Hansen, K. S. and Dial, K. P. (2007). Does the metabolic rate–flight speed relationship vary among geometrically similar birds of different mass? *J. Exp. Biol.* **210**, 1075-1083.

Daley, M. A. and Biewener, A. A. (2003). Muscle force-length dynamics during level *versus* incline locomotion: a comparison of *in vivo* performance of two guinea fowl ankle extensors. *J. Exp. Biol.* **206**, 2941-2958.

Dial, K. P. (1992). Activity patterns of the wing muscles of the pigeon (*Columba livia*) during different modes of flight. *J. Exp. Zool.* **262**, 357-373.

Dial, K. P. and Biewener, A. A. (1993). Pectoralis muscle force and power output during different modes of flight in pigeons (*Columba livia*). *J. Exp. Biol.* **176**, 31-54.

Dudley, R. and Ellington, C. P. (1990). Mechanics of forward flight in bumblebees. I. Kinematics and morphology. *J. Exp. Biol.* **148**, 19-52.

Dutto, D. J., Hoyt, D. F., Cogger, E. A. and Wickler, S. J. (2004). Ground reaction forces in horses trotting up an incline and on the level over a range of speeds. *J. Exp. Biol.* **207**, 3507-3514.

Ellington, C. P. (1984). The aerodynamics of hovering insect flight. V. A vortex theory. *Philos. Trans. R. Soc. Lond. B Biol. Sci.* **305**, 115-144.

Gabaldon, A. M., Nelson, F. E. and Roberts, T. J. (2004). Mechanical function of two ankle extensors in wild turkeys: shifts from energy production to energy absorption during incline *versus* decline running. *J. Exp. Biol.* **207**, 2277-2288.

Gillis, G. B. and Biewener, A. A. (2002). Effects of surface grade on proximal hindlimb muscle strain and activation during rat locomotion. *J. Appl. Physiol.* **93**, 1731-1743.

Gottschall, J. S. and Kram, R. (2005). Ground reaction forces during downhill and uphill running. *J. Biomech.* **38**, 445-452.

Hatze, H. (1988). High-precision three-dimensional photgrammetric calibration and object space reconstruction using a modified DLT approach. *J. Biomech.* **21**, 533-538.

Hedrick, T. L., Usherwood, J. R. and Biewener, A. A. (2004). Wing inertia and whole-body acceleration: an analysis of instantaneous aerodynamic force production in cockatiels (*Nymphicus hollandicus*) flying across a range of speeds. *J. Exp. Biol.* **207**, 1689-1702.

Higham, T. E. and Jayne, B. C. (2004). *In vivo* muscle activity in the hindlimb of the arboreal lizard, *Chamaeleo calyptratus*: general patterns and the effects of incline. *J. Exp. Biol.* **207**, 249-261.

Iversen, J. R. and McMahon, T. A. (1992). Running on an incline. *J. Biomech. Eng.* **114**, 435-441.

Norberg, U. M. (1990). *Vertebrate Flight*. Berlin: Springer-Verlag.

Pennycuick, C. J. (1968a). Power requirements for horizontal flight in the pigeon (*Columba livia*). *J. Exp. Biol.* **49**, 527-555.

Pennycuick, C. J. (1968b). A wind-tunnel study of gliding flight in the pigeon *Columba livia*. *J. Exp. Biol.* **49**, 509-526.

Pennycuick, C. J. (1975). Mechanics of Flight. In *Avian Biology*. Vol. V (ed. D. S. Farner and J. R. King), pp. 1-75. New York: Academic Press.

Rayner, J. M. V. (1979). A new approach to animal flight mechanics. *J. Exp. Biol.* **80**, 17-54.

Rayner, J. M. V. (1999). Estimating power curves of flying vertebrates. *J. Exp. Biol.* **202**, 3449-3461.

Rice, W. R. (1989). Analyzing tables of statistical tests. *Evolution* **43**, 223-225.

Roberts, T. J. and Belliveau, R. A. (2005). Sources of mechanical power for uphill running in humans. *J. Exp. Biol.* **208**, 1963-1970.

Rothe, H. J., Biesel, W. and Nachtigall, W. (1987). Pigeon flight in a wind tunnel. *J. Comp. Physiol. B* **157**, 99-109.

Rubenson, J., Henry, H. T., Dimoulas, P. M. and Marsh, R. L. (2006). The cost of running uphill: linking organismal and muscle energy use in guinea fowl (*Numida meleagris*). *J. Exp. Biol.* **206**, 2395-2408.

Soman, A., Hedrick, T. L. and Biewener, A. A. (2005). Regional patterns of pectoralis fascicle strain in the pigeon *Columba livia* during level flight. *J. Exp. Biol.* **208**, 771-786.

Stepniewski, W. Z. and Keys, C. N. (1984). *Rotary-wing Aerodynamics*. New York: Dover Publications.

Tobalske, B. W. and Dial, K. P. (1996). Flight kinematics of black-billed magpies and pigeons over a wide range of speeds. *J. Exp. Biol.* **199**, 263-280.

Tobalske, B. W., Hedrick, T. L., Dial, K. P. and Biewener, A. A. (2003). Comparative power curves in bird flight. *Nature* **421**, 363-366.

Tobalske, B. W., Warrick, D. R., Clark, C. J., Powers, D. R., Hedrick, T. L., Hyder, G. and Biewener, A. A. (2007). Three-dimensional kinematics of hummingbird flight. *J. Exp. Biol.* **210**, 2368-2382.

Torre-Bueno, J. R. and Larochelle, J. (1978). The metabolic cost of flight in unrestrained birds. *J. Exp. Biol.* **75**, 223-229.

Usherwood, J. R. and Ellington, C. P. (2002a). The aerodynamics of revolving wings. II. Propeller force coefficients from mayfly to quail. *J. Exp. Biol.* **205**, 1565-1576.

Usherwood, J. R. and Ellington, C. P. (2002b). The aerodynamics of revolving wings. I. Model hawkmoth wings. *J. Exp. Biol.* **205**, 1547-1564.

Usherwood, J. R., Hedrick, T. L., McGowan, C. P. and Biewener, A. A. (2005). Dynamic pressure maps for wings and tails of pigeons in slow, flapping flight, and their energetic implications. *J. Exp. Biol.* **208**, 355-369.

Wakeling, J. M. and Ellington, C. P. (1997a). Dragonfly flight. II. Velocities, accelerations and kinematics of flapping flight. *J. Exp. Biol.* **200**, 557-582.

Wakeling, J. M. and Ellington, C. P. (1997b). Dragonfly flight. III. Lift and power requirements. *J. Exp. Biol.* **200**, 583-600.